

FINDING THE ELECTROMAGNETIC COUNTERPARTS OF COSMOLOGICAL STANDARD SIRENS

BENCE KOCSIS

Institute of Physics, Eötvös University, Pázmány P. s. 1/A, 1117 Budapest, Hungary; bkocsis@complex.elte.hu

ZSOLT FREI

Institute of Physics, Eötvös University, Pázmány P. s. 1/A, 1117 Budapest, Hungary; frei@alcyone.elte.hu

ZOLTÁN HAIMAN

Department of Astronomy, Columbia University, 550 West 120th Street, New York, NY 10027; zoltan@astro.columbia.edu

KRISTEN MENOUE

Department of Astronomy, Columbia University, 550 West 120th Street, New York, NY 10027; kristen@astro.columbia.edu

Accepted for publication in ApJ

ABSTRACT

The gravitational waves (GW) emitted during the coalescence of supermassive black holes (SMBHs) in the mass range $\sim (10^4 - 10^7) M_{\odot} / (1+z)$ will be detectable out to high redshifts with the future *Laser Interferometric Space Antenna (LISA)*. The distance and direction to these “standard sirens” can be inferred directly from the GW signal, with a precision that depends on the masses, spins and geometry of the merging system. In a given cosmology, the *LISA*-measured luminosity distance translates into a redshift shell. We calculate the size and shape of the corresponding three-dimensional error volume in which an electromagnetic counterpart to a *LISA* event could be found, taking into account errors in the background cosmology (as expected by the time *LISA* flies), weak gravitational lensing (de-)magnification due to inhomogeneities along the line of sight, and potential source peculiar velocities. Weak lensing errors largely exceed other sources of uncertainties (by a factor of ~ 7 for typical sources at $z = 1$). Under the plausible assumption that SMBH-SMBH mergers are accompanied by gas accretion leading to Eddington-limited quasar activity, we then compute the number of quasars that would be found in a typical three-dimensional *LISA* error volume, as a function of BH mass and event redshift. Low redshifts offer the best opportunities to identify quasar counterparts to cosmological standard sirens. For mergers of $\sim (4 \times 10^5 - 10^7) M_{\odot}$ SMBHs, the *LISA* error volume will typically contain a single near-Eddington quasar at $z \sim 1$. If SMBHs are spinning rapidly, the error volume is smaller and may contain a unique quasar out to redshift $z \sim 3$. This will allow a straightforward test of the hypothesis that GW events are accompanied by bright quasar activity and, if the hypothesis proves correct, will guarantee the identification of a unique quasar counterpart to a *LISA* event, with a B-band luminosity of $L_B \sim (10^{10} - 10^{11}) L_{\odot}$. Robust counterpart identifications would allow unprecedented tests of the physics of SMBH accretion, such as precision-measurements of the Eddington ratio. They would clarify the role of gas as a catalyst in SMBH coalescences, and would also offer an alternative method to constrain cosmological parameters.

Subject headings: cosmology: theory – cosmology: observations – large scale structure of universe – cosmic microwave background – galaxies: clusters: general

1. INTRODUCTION

One of the main objectives of the *Laser Interferometric Space Antenna (LISA)*, to be launched around the year 2013 (Danzmann 2004), is to detect the gravitational wave (GW) signals associated with coalescing supermassive black holes (SMBH) at cosmological distances. The *LISA* detector is designed to be particularly sensitive in the frequency range between $(3 \times 10^{-5} - 10^{-4}) \text{ Hz} \lesssim f \lesssim 0.1 \text{ Hz}$, allowing the detection of binary coalescences with total masses between 10^4 and $10^7 M_{\odot}$ out to high redshifts. The limiting redshift depends on several factors (such as the orientation of the spins and orbital plane of the SMBH binary, and its location on the sky relative to *LISA*), and is expected to lie between $z \sim 5 - 10$ (Hughes 2002). A comparison of the gravitational waveform with the anticipated detector noise can be used to estimate the accuracy with which *LISA* will be able to extract the physical parameters of the coalescence events (Hughes 2002; Barack & Cutler 2004; Vecchio 2004; Holz & Hughes 2005).

Of particular interest, in the context of searching for electromagnetic (EM) counterparts, is whether the spatial location of the GW event can be localized to within a sufficiently small three-dimensional volume. In this paper, we determine the probability of finding a unique EM counterpart within the expected error volume associated with SMBH merger events, for a range of masses and redshifts.

It has been argued by Vecchio (2004) that the identification of such EM counterparts will be difficult because, in typical cases, there will be too many counterpart candidates to choose from. However, Vecchio (2004) associated counterparts with host galaxies and galaxy clusters, and used only the 2D angular positioning information for the analysis. In contrast, here we account for the 3D spatial information by using the redshift of an electromagnetic counterpart candidate in relation with the luminosity distance determined by *LISA* and we focus on quasars as plausible counterparts. With these specifications, we shall demonstrate that in some cases, a specific counterpart can be uniquely determined.

If electromagnetic counterparts to *LISA* events exist, they will likely be related to the accretion of gas onto the SMBHs involved in the coalescence. Provided this accretion is not supply-limited, bright quasar counterparts approaching the Eddington luminosity would then be expected. A few additional arguments favor this scenario: galaxy mergers in hierarchical scenarios of structure formation are expected to deliver a significant amount of gas to the central regions of the merging galaxies (Barnes & Hernquist 1992), and this gas may play a catalyst role in driving SMBH coalescence (Begelman, Blandford, & Rees 1980; Gould & Rix 2000; Escala et al. 2004). Ultimately, however, many of the complex processes involved remain poorly understood. For example, Armitage & Natarajan (2002) have argued that, in the limit of a small mass ratio of the two SMBHs, a prompt and luminous electromagnetic signal may be expected during coalescence, while Milosavljevic & Phinney (2005) have argued that in the limit of equal mass SMBHs, only a much delayed electromagnetic afterglow would be expected. All “cosmological standard sirens” may thus not be equal in their potential for electromagnetic counterparts.¹ Our working assumption in the present study is that bright quasar activity is a plausible electromagnetic counterpart to *LISA* events. This allows us to quantify the feasibility of an unambiguous identification of such a counterpart. As we shall see below, the search for the counterparts will allow a test of the assumption, as well.

The secure identification of the EM counterpart to even a single GW event could be useful in different ways: (1) to improve our understanding of the SMBH accretion physics, (2) to clarify the role of gas as a catalyst in SMBH mergers and (3) to supply an independent constraint on the background cosmology. A joint GW – EM analysis could, in principle, determine the masses and orbital parameters of the SMBH binary, and yield a precise measurement of the Eddington ratio, L/L_{Edd} , which will supply a key parameter in studies of the evolution of the BH/quasar population (Small & Blandford 1992; Haiman & Loeb 1998; Kauffmann & Haehnelt 2000; Haiman & Menou 2000; Wyithe & Loeb 2003). This parameter is currently poorly known (constrained by indirect empirical correlations; Vestergaard 2004, Woo & Urry 2002, Kaspi et al. 2000). The values range from ≈ 0.1 to $\gtrsim 1$, with indications that higher- z quasars may be closer to L_{Edd} than the $z \sim 0$ quasars. Likewise, a joint GW – EM analysis could, in principle, be used to estimate cosmological parameters (Schutz 1986), by comparing the luminosity distance (which is a direct observable by GWs) with the redshift (as inferred from the spectrum of the counterpart – in this case, a quasar). This would serve as a complement to constraints from the luminosity distance to high- z type Ia Supernovae (SNe), but with different systematic errors, and with the potential of extending to higher redshifts. New constraints, spanning the range $0 < z < 2$, would be particularly well-suited to probe the properties of dark energy, which is expected to become dynamically dominant within this cosmic epoch.

The rest of this paper is organized as follows. In § 2, we summarize our method to estimate the angular and radial positioning errors expected from *LISA*, for SMBHs with a range of masses at different redshifts. In § 3, we discuss the conversion of the luminosity distance, as determined by *LISA* from the GW signal alone, to the redshift of the source. In

TABLE 1
LISA MEASUREMENT ERRORS

	$\delta\mathcal{M}/\mathcal{M}$	$\delta\mu/\mu$	$\delta d_L/d_L$	$\delta\Omega$
best	0.8×10^{-5}	2×10^{-5}	2×10^{-3}	0.01 deg^2
typical	2×10^{-5}	9×10^{-5}	4×10^{-3}	0.3 deg^2
worst	0.8×10^{-3}	0.1	2×10^{-2}	3 deg^2

NOTE. — Assumed SMBH binary parameters: $m_1 = m_2 = 10^6 M_\odot$ and $z = 1$.

particular, we discuss the uncertainty in the resulting redshift estimate. In § 4, we discuss our estimates for the number of quasars that may be found in the 3D error volume provided by *LISA*, based on the luminosity function and clustering properties of known optical quasars. In § 5, we present our main results, and show that for typical low-redshift GW events discovered by *LISA*, a unique quasar counterpart may be identified. In § 6, we point out various implications of a successful identification and discuss several caveats to this conclusion. Finally, in § 7 we summarize our conclusions. Unless stated otherwise, throughout this paper we assume a standard cold-dark matter cosmology (Λ CDM), with $(\Omega_\Lambda, \Omega_M, \Omega_b, H_0) = (0.70, 0.30, 0.047, 70 \text{ km s}^{-1} \text{ Mpc}^{-1})$, consistent with the recent results from the *Wilkinson Microwave Anisotropy Probe* (*WMAP*) (Spergel et al. 2003) and the Sloan Digital Sky Survey (SDSS) (Tegmark et al. 2004).

2. LOCALIZING *LISA* EVENTS

A few studies have been carried out so far to address how accurately *LISA* will measure the source parameters of a coalescing pair of SMBHs. In general, the accuracy depends on a large number of parameters: a total of 17 parameters in the most general case include 2 red-shifted mass parameters, 6 parameters related to the BH spin vectors, the orbital eccentricity, the luminosity distance, 2 angles identifying the position on the sky, 3 angles that describe the orientation of the orbit, a reference time, and a reference phase. Due to the resulting computational limitations, various studies have concentrated on small portions of the parameter space. The most up-to-date calculations estimating parameter uncertainties for SMBH in-spirals have been carried out by Berti, Buonanno, & Will (2005a); Holz & Hughes (2005); and by Vecchio (2004). As compared to previous studies, Vecchio (2004) accounts for the effects of spins, and shows that parameter estimation errors improve significantly (by a factor of 3–10 for high spins) for selected parameters. Vecchio (2004) also adopts an optimistic *LISA* sensitivity curve, by adopting the smallest observable frequency to be ~ 3 times lower than previous estimates and only considers cases with equal mass SMBHs. Our analysis, which relies on Vecchio’s estimates, is therefore approximate to this extent.

For concreteness, we adopt the parameter uncertainties obtained by Vecchio (2004) for an equal-mass SMBH binary with $m_1 = m_2 = 10^6 M_\odot$ at redshift $z = 1$. The uncertainties vary as a function of the fiducial orientation of the source relative to *LISA*, and are primarily influenced by the BH spin magnitudes (i.e. higher spins lead to smaller uncertainties). Here we distinguish three cases. For our “best” case, we adopt the errors that correspond to the 10th percentile of the distribution of uncertainties obtained by Vecchio (2004) for high BH spins (with dimensionless spin $a = S/M^2 = 0.9$, where S is the magnitude of the total spin and M is the total mass). For our

¹ The name “standard sirens” was suggested by Sterl Phinney and Sean Carroll (Holz & Hughes 2005).

“typical” case, we adopt the errors corresponding to the 50th percentile in the case of moderate BH spins, with $a = 0.5$. For our “worst” case, we adopt the 90th percentile of the no spin case ($a = 0$). Note that SMBHs are generally expected to be spinning fast (e.g. Volonteri et al. 2005), so that our “best” case may actually be representative of a fair fraction of events. In Table 1, we list the errors on the chirp and reduced masses, $\mathcal{M} = (m_1 m_2)^{3/5} / (m_1 + m_2)^{1/5}$ and $\mu = (m_1 m_2) / (m_1 + m_2)$ respectively, and on the GW source location (i.e. luminosity distance, d_L , and solid angle, Ω), for these three cases of interest.

In Vecchio (2004), parameter errors have only been estimated for a single choice of an equal-mass SMBH binary with total mass $M_0 = m_1 + m_2 = 2 \times 10^6 M_\odot$ and redshift $z_0 = 1$. Starting from this result, we crudely estimate the uncertainties δd_L and $\delta \Omega$ for other combinations of masses and redshifts as follows. First, note that the luminosity distance is simply proportional to the inverse of the signal amplitude. Therefore its estimator depends primarily on the total signal power, rather than on the specific shape of the signal waveform². The luminosity distance error would then obey the simple scaling

$$\frac{\delta d_L(M, z)}{d_L(M, z)} = \left[\frac{SNR(M, z)}{SNR(M_0, z_0)} \right]^{-1} \frac{\delta d_L(M_0, z_0)}{d_L(M_0, z_0)} \quad (1)$$

where $SNR(M, z)$ is the expected value of the signal to noise ratio of the detection,

$$SNR^2(M, z) = 4 \int_{f_a(M_z, \Delta T)}^{f_{isco}(M_z)} \frac{h^*(f, M_z, z) h(f, M_z, z)}{S_n(f)} df. \quad (2)$$

Here, $M_z = (1+z)M$ is the red-shifted total mass, $h(f, M_z, z)$ denotes the Fourier decomposition of the signal detected by *LISA*, and $S_n(f)$ is the RMS noise density per frequency interval (including instrumental and confusion noise, Barack & Cutler 2004³). A crucial parameter for high M_z values inscribed in $S_n(f)$ is the low frequency wall of the detector, which is further discussed below. The integration bound $f_{isco}(M_z)$ corresponds to the innermost stable circular orbit (ISCO), beyond which the gravitational waveform is not well known, and $f_a(M_z, \Delta T)$ is the arrival frequency a time ΔT before the ISCO is reached by the coalescing binary (see Vecchio 2004 for details). Throughout this paper, we fix the observation time of SMBH binaries at $\Delta T = 1$ yr, unless a binary is so massive or at such a high redshift that it is not observable by *LISA* for a full year and then $\Delta T < 1$ yr. Note that $h(f, M_z, z)$ depends on other parameters, such as the angular momentum vector orientation relative to *LISA*’s arms, the magnitude of spins, etc. (see Vecchio 2004 and references therein). For this estimate we calculate the SNR with the leading order (i.e. Newtonian) contribution. The resulting dependence of the signal-to-noise ratio on BH masses and redshift are shown in Figure 1. The figure shows that the sensitivity degrades significantly for distant sources, and also that it peaks in the mass range of $10^5 - 10^6 M_\odot$, which produce GWs near the optimal frequencies within the *LISA* band.

The other important parameter, the angular position, is extracted from the change in the relative orientation of *LISA* during its orbit around the Sun. Since *LISA*’s orbital time-scale

² The signal power also scales with the red-shifted chirp mass as $\mathcal{M}_z^{5/6}$. However, this parameter can be determined independently to high precision, from the phase information.

³ For the instrumental noise, instead of the approximation of Barack & Cutler (2004), we use the more exact sensitivity curve available at <http://www.srl.caltech.edu/~shane/sensitivity/>.

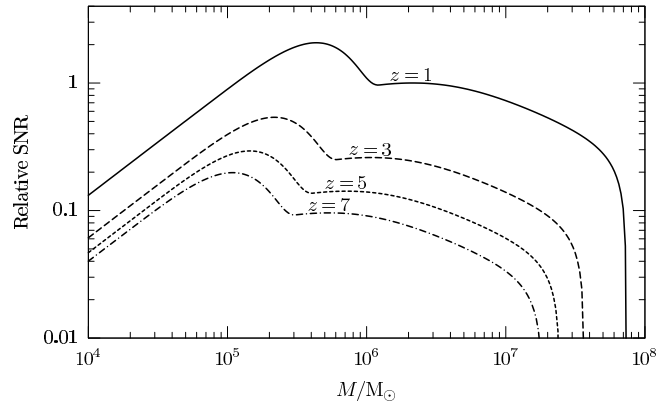


FIG. 1.— Relative signal-to-noise ratio (SNR) for *LISA* detections of the in-spiral phase of equal-mass supermassive black hole coalescences, as a function of total mass, M , and redshift, z . A 1-year observation is assumed and the normalization is for $M = 2 \times 10^6 M_\odot$ and $z = 1$.

is much longer than the inverse of the signal frequency, it is plausible to assume that the angular position uncertainty decouples from the intricate waveform, and improves linearly with the signal amplitude. This assumption is consistent with Fig. 1 of Berti, Buonanno, & Will (2005b) which shows that the inclusion of spin-orbit and spin-spin terms modifies the waveforms but does not alter the angular resolution. In fact, the angular resolution is shown to be independent even for alternate theories of gravity (e.g. scalar-tensor and massive graviton theories). Thus, similar to equation (1), we estimate the mass and redshift dependence of the positioning solid-angle error as

$$\delta \Omega(M, z) = \left[\frac{SNR(M, z)}{SNR(M_0, z_0)} \right]^{-2} \delta \Omega(M_0, z_0), \quad (3)$$

where the -2 exponent assumes that the uncertainty in this two-dimensional quantity is the product of independent uncertainties in the one-dimensional azimuthal and polar angles.

A limitation of the above analysis at the high-mass end of the range of SMBHs is that these events may not be visible for a full year, due to the low-frequency noise wall, below which *LISA* loses sensitivity. For instance, for $M_z > 9 \times 10^6 M_\odot$ ($1.3 \times 10^6 M_\odot$), the low frequency noise wall at 0.03mHz (0.1mHz) is crossed less than 0.25yr before reaching the ISCO. At higher masses or redshifts, therefore, the angular information, which is inscribed in a modulation with a 1yr period, becomes significantly harder to disentangle from other parameters, such as d_L , and the errors estimated from the SNR alone by equations (1) and (3) become less accurate. In this regime, a better approximation to the scaling of the errors is $\propto (\Delta T / 1 \text{ yr})^{-1/2} \times SNR^{-1}$, where $\Delta T \leq 1$ yr is the time elapsed from the moment the binary appears at the low-frequency wall to the moment it reaches the ISCO (Hughes 2005, private communication; see Holz & Hughes (2005) for a more detailed treatment and discussion).

3. LOCALIZING THE COUNTERPARTS

We next consider how to use the three-dimensional spatial localization of the SMBH merger event by *LISA*. The solid angle error box directly yields the two-dimensional angular position error on the sky, in which any EM counterpart will be located. However, an additional step is necessary to convert the luminosity distance, d_L , measured by *LISA* into a redshift, z , which is the relevant observable for the EM coun-

terpart. With a particular choice of cosmological parameters $p_i = (H_0, \Omega_M, \Omega_{DE}, w)$, we can directly convert a redshift to a luminosity distance (see eq. 4 below), and vice-versa. One may then envision the following strategy: given the precision with which p_i are known from other observations, one can estimate the redshift, and restrict the search for counterparts within the redshift shell corresponding to the *LISA*-measured luminosity distance, d_L . If a counterpart is uniquely identified within this redshift shell, and its redshift can be determined precisely, then one could hope for an improved measurement of the $d_L(z)$ relation, and hence a refined determination of the cosmological parameters.

The first step in this exercise is to determine the expected redshift of the source. Apart from the errors on the cosmological parameters and on the measurement of d_L , the peculiar velocity of the source relative to the Hubble flow, and its magnification due to weak gravitational lensing by inhomogeneities in the distribution of mass along the line of sight, introduce two additional sources of errors. In summary, the redshift uncertainty will thus include a combination of uncertainties from (i) the *LISA* luminosity distance, (ii) the cosmological parameters, (iii) peculiar velocities, and (iv) weak gravitational lensing magnification.

Hughes (2002) made a simplified estimate of the redshift error, without peculiar velocities or gravitational lensing distortions, assuming a flat cosmology with a cosmological constant (assuming $\Omega_M \equiv 1 - \Omega_\Lambda$ and $w \equiv -1$), and ignoring correlations with other cosmological parameters. Here, we extend that study by using a general form of dark energy (relaxing the w prior), by taking into account the various parameter correlations, and by including errors due to peculiar velocities and gravitational lensing.

To begin, we recall the luminosity distance to a source at a fixed comoving coordinate in a smooth Friedmann universe,

$$d_L(z, p_i) = (1+z)c \int_0^z \frac{dz'}{H(z', p_i)}, \quad (4)$$

where

$$H(z, p_i) = H_0 \sqrt{\Omega_M(1+z)^3 + \Omega_{DE}(1+z)^{3(1+w)}}. \quad (5)$$

We ignore spatial curvature and set $\Omega_k = 0$, in line with previous studies and as suggested by recent *WMAP* data. For a source with a small but non-zero radial peculiar velocity, v , equation (4) is modified, and the luminosity distance is given by

$$d_L(z, p_i, v) = d_L[z_v, p_i, 0], \quad (6)$$

where $\Delta z \equiv z_v - z = (1+z)v/c$ is the additional apparent redshift due to the peculiar motion. In an inhomogeneous universe, sources along different lines of sight can suffer different amounts of gravitational lensing magnification μ . If μ denotes the magnification of the signal power, then the GW amplitude, and thus the inferred value of d_L^{-1} , scales as $\mu^{1/2}$. For a line of sight that suffers a magnification μ , equation (6) is modified as

$$d_L(z, p_i, v, \mu) = \frac{1}{\sqrt{\mu}} d_L[z_v, p_i, 0]. \quad (7)$$

In the limit of weak lensing $\mu^{1/2} \simeq 1 + \kappa$, where $\kappa \ll 1$ denotes the weak lensing convergence (see below).

Taking the variation in both sides of equation (7), we obtain

$$\delta d_L = -d_L \kappa + \frac{\partial d_L}{\partial z} \delta z + \frac{\partial d_L}{\partial v} v + \sum_i \frac{\partial d_L}{\partial p_i} \delta p_i, \quad (8)$$

Solving for δz , taking the square and the expectation value of both sides, and using the fact that the *LISA* measurement, the peculiar velocities, and the cosmological uncertainties are independent, i.e. $\langle \delta p_i \delta d_L \rangle = \langle v \delta d_L \rangle = \langle \kappa \delta d_L \rangle = \langle v \delta p_i \rangle = \langle \kappa \delta p_i \rangle = \langle \kappa v \rangle = 0$ for all i , we find

$$\langle \delta z^2 \rangle = \left(\frac{\partial d_L}{\partial z} \right)^{-2} (\langle \delta d_{L, \text{LISA}}^2 \rangle + \langle \delta d_{L, \text{cosm}}^2 \rangle + \langle \delta d_{L, \text{pec}}^2 \rangle + \langle \delta d_{L, \text{wl}}^2 \rangle) \quad (9)$$

or equivalently,

$$\langle \delta z^2 \rangle = \langle \delta z_{\text{LISA}}^2 \rangle + \langle \delta z_{\text{cosm}}^2 \rangle + \langle \delta z_{\text{pec}}^2 \rangle + \langle \delta d_{\text{wl}}^2 \rangle, \quad (10)$$

where the notation was introduced to distinguish the intrinsic *LISA* measurement error, $\delta d_{L, \text{LISA}}$, from the error resulting from cosmological parameters $\langle \delta d_{L, \text{cosm}}^2 \rangle$, peculiar velocities $\langle \delta d_{L, \text{v}}^2 \rangle$, and weak lensing magnification $\langle \delta d_{L, \text{wl}}^2 \rangle$. We now discuss each of these terms, whose forms and magnitudes follow directly from equation (7).

3.1. Cosmological uncertainties

The cosmological term in equation (9) is

$$\langle \delta d_{L, \text{cosm}}^2 \rangle = \sum_{i,j} \frac{\partial d_L}{\partial p_i} \frac{\partial d_L}{\partial p_j} \langle \delta p_i \delta p_j \rangle, \quad (11)$$

where d_L and its derivatives are to be evaluated using equation (4), at the fiducial values of the cosmological parameters p_i , and for $v = \kappa = 0$. In order to place *LISA* in the context of other experiments planned in the next decade, we compute $\langle \delta d_{L, \text{cosm}}^2 \rangle$ from the covariance matrices $\langle \delta p_i \delta p_j \rangle$ expected from two future cosmological probes: *Planck*⁴ (assumed to have measured the temperature and polarization anisotropies of the cosmic microwave background), and the Large Synoptic Survey Telescope, LSST⁵ (assumed to have measured the power spectrum and redshift distribution of $\sim 100,000$ galaxy clusters). We adopt the forecasts for the Fisher matrices for these experiments by Wang et al. (2004). Their analysis assumes a flat background universe with 6 free parameters $(\Omega_{DE}, \omega_M, w, \omega_b, n_s, \sigma_8)$ where $\omega_M \equiv \Omega_M h^2 \equiv (1 - \Omega_{DE}) h^2$ defines the Hubble parameter. Note that the luminosity distance does not explicitly depend on n_s and σ_8 , but they are included here, since they couple to the other four parameters as determined by *Planck* and LSST (and hence increase the uncertainties on these other four parameters). The fiducial parameters are (0.73, 0.14, -1, 0.024, 1, 0.9), respectively (consistent with *WMAP*; Spergel et al. 2003). Since the two observations are independent, we simply sum up the two individual Fisher matrices; the covariance matrix, $\langle \delta p_i \delta p_j \rangle$, is obtained by taking the inverse of the Fisher matrix. In order to substitute in equation (11), it is necessary either to revert to the original cosmological parameters $(H_0, \Omega_{DE}, \Omega_M, w)$ in the correlation matrix, by performing an orthogonal transformation in the parameter space⁶, or to simply write $d_L(z, p_i)$ of equation (4) in terms of the parameters $(\Omega_{DE}, \omega_m, w)$ and evaluate the partial derivatives in equation (11) as a function of these parameters. Following either approach, we find $\langle \delta d_{L, \text{cosm}}^2 \rangle^{1/2} / d_L = 1.7 \times 10^{-3}$ for $z = 1$. For comparison, we performed the same analysis using the Fisher matrices of *WMAP* (using only temperature anisotropies) and SDSS (using the power spectrum

⁴ See www.rssd.esa.int/index.php?project=PLANCK

⁵ See www.lsst.org

⁶ The parameters $\delta \Omega_M$ and $\delta \Omega_{DE}$ will be fully anti-correlated, because of the assumption of flatness.

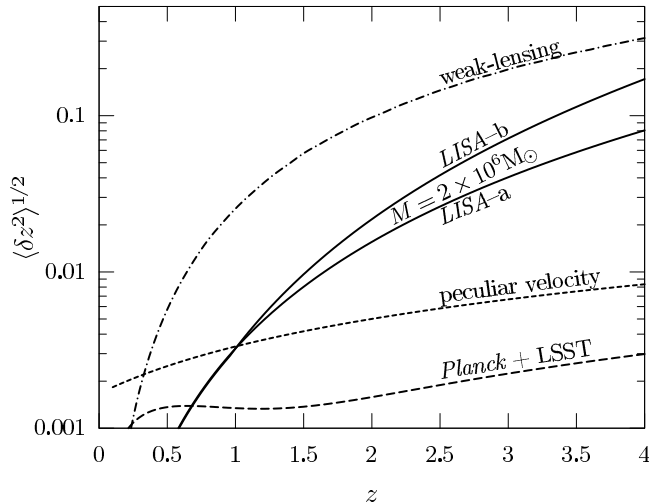


FIG. 2.— Errors on the inferred redshift of an electromagnetic counterpart to a *LISA* coalescence event, for $m_1 = m_2 = 10^6 M_\odot$. The intrinsic *LISA* error on the luminosity distance, d_L , is shown as a solid line for the two scalings $\delta d_L/d_L \propto SNR^{-1}$ (“*LISA*-a”) and $\delta d_L/d_L \propto \Delta T^{-1/2} \propto SNR^{-1}$ (“*LISA*-b”). Errors due to the peculiar velocity of the source (for $v = 500 \text{ km s}^{-1}$; short-dashed line), uncertainties on the background cosmology (long-dashed line), and weak lensing magnification (dash-dotted line) are also shown (see text for details).

of the luminous red galaxies, together with the galaxies in the main SDSS survey, and following Hu & Haiman 2003 for redshift binning, mass limit, and sky coverage). We find $\langle \delta d_{L,\text{cosm}}^2 \rangle^{1/2}/d_L = 1.1 \times 10^{-2}$ for $z = 1$ in that case.

The luminosity distance error corresponds to a redshift error according to equation (9). Note that equation (11) depends on the fiducial redshift through the d_L derivatives. This dependence of the redshift error is shown as a long-dashed curve in Figure 2, along with other sources of redshift errors. The luminosity distance at $z \approx 1000$ is measured very accurately by *Planck*, and its evolution is essentially unaffected by the cosmological parameters down to dark-energy domination at $z \lesssim 2$. The figure shows that, as a result, the relative cosmological error $\langle \delta z_{\text{cosm}}^2 \rangle^{1/2}/z$ reaches a constant value beyond $z \gtrsim 2$. The figure also shows that the cosmology error becomes smaller than the typical *LISA* uncertainty at $z \gtrsim 0.7$. We find that, even for our best-case *LISA* events, the cosmology error becomes sub-dominant at $z \gtrsim 1$.

3.2. Peculiar velocities

Equations (6), (8), and (9) yield, to first non-vanishing order in v/c , the uncertainty due to peculiar velocities, as a simple function of the r.m.s. peculiar velocity of the GW sources,

$$\langle \delta d_{L,\text{pec}}^2 \rangle / d_L^2 = \left[1 + \frac{c(1+z)^2}{H(z)d_L} \right]^2 \frac{\langle v^2 \rangle}{c^2}. \quad (12)$$

We are assuming here that GW events correspond to luminous quasars, and unfortunately, the r.m.s. peculiar velocity of high-redshift quasars is not known empirically. We therefore employ theoretical predictions for the peculiar velocities of (quasar–host) galaxies within dark matter haloes. According to numerical simulations (e.g. Cen & Ostriker 2000), typical values are $\sim 500 \text{ km s}^{-1}$, with a tail extending to $\sim 1000 \text{ km s}^{-1}$. As an approximation, we assume that the scaling with redshift follows the linear growth in the amplitude of

density perturbations, multiplied by the linear bias of the halos. Under this assumption, we find that for fixed halo mass, the typical peculiar velocity evolves very little from $z \sim 0$ to $z \sim 1$. This conclusion is consistent with the semi-analytic model of Hamana et al. (2003), which shows essentially no evolution (only a modest decrease from $z \sim 0$ to $z \sim 0.8$). Therefore, we substitute $v \sim 500 \text{ km s}^{-1}$ in equation (12) at $z \sim 1$, yielding an error of $\langle \delta d_{L,\text{pec}}^2 \rangle^{1/2}/d_L = 4.1 \times 10^{-3}$. The corresponding redshift r.m.s. error contribution (equation [10]) for $v \sim 500 \text{ km s}^{-1}$ is shown as a function of redshift in Figure 2 (short-dashed curve). The figure shows that the peculiar velocity error is lower than the typical *LISA* error for $z \gtrsim 1$.

Note that the r.m.s. peculiar velocity equals $\sim 500 \text{ km s}^{-1}$ in the most typical cases, but its exact value depends on the specific mass of the halo, M_{halo} , embedding the quasar (Hamana et al. 2003), smaller M_{halo} implying lower velocities. For a specific source, M_{halo} can be estimated directly, using the number of galaxies that cluster around the identified quasar (Kauffmann & Haehnelt 2002). The r.m.s. peculiar velocity error may then be estimated for this particular source, and may be somewhat lower/higher than the value shown in Figure 2, depending on whether the source is located in a galaxy-poor/galaxy-rich environment.

3.3. Weak Gravitational Lensing

The gravitational lensing term in equation (9), in the weak-lensing limit, is given by

$$\langle \delta d_{L,\text{wl}}^2 \rangle / d_L^2 = \langle \kappa^2 \rangle, \quad (13)$$

where κ denotes the r.m.s. effective convergence (e.g., White & Hu 2000). While the mean magnification is well approximated by $\langle \kappa \rangle = 0$ or $\langle \mu \rangle = 1$, the magnification distribution has a substantial width. The full distribution is given by Wang, Holz, & Munshi (2002), and its variance reaches $\sim 12\%$ for sources at $z = 2$ (Dalal et al. 2003). Here we use equation (6) in White & Hu (2000) to compute the variance in effective convergence, $\langle \kappa^2 \rangle$, for point sources. This quantity is given by an integral over the matter power spectrum, and receives a contribution from small, non-linear scales. We employ the HALOFIT routine of Smith et al. (2003), and set the input cosmological parameters according to our convention (see § 1). This routine encodes an accurate fitting formula for the matter power spectrum extending into the nonlinear regime. For $z = 1$, we find $\langle \kappa^2 \rangle^{1/2} = 3.1\%$.

Weak lensing errors can, in principle, be improved by “corrective lenses” (Dalal et al. (2003)), i.e. background galaxy shear maps, and using the cross-correlation between the magnification of a point source and the shear map smoothed on larger-scales. However, Dalal et al. (2003) found that the magnification errors can be improved by only a small amount, less than 20% relative to the uncorrected errors for a source at $z = 2$.

A different approach for reducing weak lensing magnification uncertainty would be to directly measure the inhomogeneities in the mass distribution along the line of sight. If this distribution could be directly probed down to a scale of k_{min} , then the contributions to κ from all scales down to k_{min} could be directly subtracted from the uncertainty on the magnification. If the counterpart is indeed a quasar, then the line-of-sight density distribution could, in principle, be probed by studying its Lyman α absorption spectrum, as well as deep surveys of galaxies and clusters in the foreground and near the

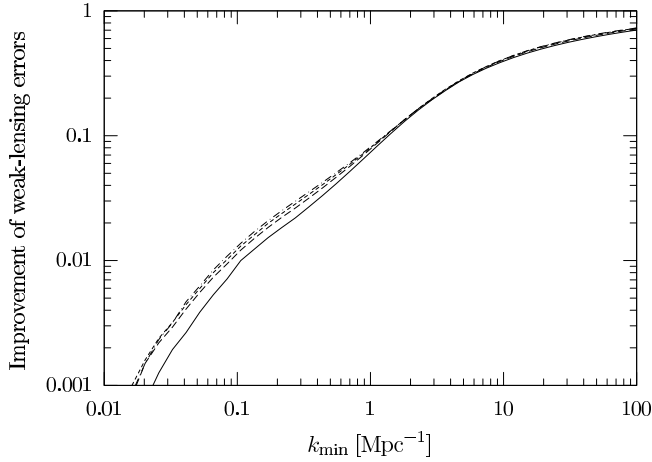


FIG. 3.— The relative improvement in the weak lensing magnification-induced redshift uncertainty to a background source. We show the fractional improvement that can be achieved by perfectly measuring density inhomogeneities down to a fixed scale. The x -axis shows the minimum wave number that is unmapped (larger scale fluctuations are assumed to be perfectly known along the line of sight to the source). Various curves correspond to sources at $z = 1, 2, 3,$ and 4 (from bottom to top).

line of sight. At low redshifts ($z \sim 0.5$) which contribute significantly to the lensing magnification, the X-ray absorption forest (Fang & Canizares 2000; Perna & Loeb 1998) could provide additional information on the density fluctuations.

We leave a detailed assessment of the amount of correction that could be feasible to future investigations. However, to estimate the “target” scale at which the fluctuations would need to be measured in order to be useful as a lensing correction, we make the (unrealistically optimistic) simplifying assumption that the matter fluctuations above a certain length scale, and the corresponding contribution to lensing magnification, have been perfectly determined. The fluctuations on smaller scales, with $k > k_{\min}$, then determine the only remaining weak-lensing uncertainty. Therefore, we truncate the integral over the wavenumber (see eq. [1] in Dalal et al. 2003) at k_{\min} . The resulting fractional improvement in $\langle \kappa^2 \rangle^{1/2}$ (which equals $\delta d_{L, \text{wl}}/d_L$) is plotted in Figure 3. The improvement is about 8%, 20%, and 40% for $k_{\min} = 1, 3,$ and 10 Mpc^{-1} , respectively - i.e., about half of the weak lensing uncertainty is from length-scales $\lesssim 2\pi/k_{\min} \sim 0.6 \text{ Mpc}$. The Lyman α transmission spectra of SDSS quasars have been used to determine the power spectrum down to scales of $k \sim 3 \text{ Mpc}^{-1}$, implying that the spectral resolution would need to be improved by a factor of ~ 3 to allow significant improvements.

The uncorrected weak-lensing redshift uncertainty $\delta z_{\text{wl}} \equiv (\partial d_L/\partial z)^{-1} \langle \delta d_{L, \text{wl}}^2 \rangle^{1/2}$ is shown in Figure 2. The plot clearly shows that weak lensing errors typically exceed 1% and dominate the other redshift errors for $z > 0.5$.

3.4. The Size and Orientation of the Error Volume

In Figure 2, we compare the contributions from four different sources of redshift errors: $\langle \delta z_{\text{LISA}}^2 \rangle^{1/2}$, $\langle \delta z_{\text{pec}}^2 \rangle^{1/2}$, $\langle \delta z_{\text{cosm}}^2 \rangle^{1/2}$, and $\langle \delta z_{\text{wl}}^2 \rangle^{1/2}$ for SMBH masses $m_1 = m_2 = 10^6 M_\odot$. Weak lensing errors are dominant for $5 \gtrsim z \gtrsim 0.5$. The *LISA* redshift error is shown for both scalings $\delta d_L/d_L \propto \text{SNR}^{-1}$ (labeled “*LISA*-a”) and $\delta d_L/d_L \propto (\Delta T/1 \text{ yr})^{-1/2} \times \text{SNR}^{-1}$ (labelled “*LISA*-b”). These curves separate for $M_z > 3.92 \times 10^6 M_\odot$, when the maximum observation time ΔT de-

creases under 1 yr. The other three sources of errors are within a factor of two of one another at $z = 1$, for typical *LISA* sources and peculiar velocities.

The total redshift uncertainty then follows from summing the uncertainties in quadrature (eq. [10]). The result for $m_1 = m_2 = 10^6 M_\odot$ and $z = 1$ is $\delta z = 2.57\%$, 2.59% , and 3.03% in the cases we labeled as best, typical, and worst, respectively. Note that we have not explicitly added an error due to the instrumental resolution of a spectrograph, because this is often much better than this value (e.g. for SDSS⁷, the redshift resolution is between 10^{-3} and 10^{-4}).

We next use these redshift uncertainties to derive the three-dimensional error volume, δV_{tot} , in which the EM counterparts need to be identified. The comoving volume corresponding to the above redshift uncertainties, combined with the solid-angle uncertainty $\langle \delta \Omega^2 \rangle^{1/2}$, is

$$\delta V_{\text{tot}} = \frac{\partial^2 V}{\partial z \partial \Omega} \langle \delta z^2 \rangle^{1/2} \langle \delta \Omega^2 \rangle^{1/2}. \quad (14)$$

Substituting the solid-angle errors from Table 1, we find $\delta V_{\text{tot}} = 2.1 \times 10^3$, 6.3×10^4 , and $7.4 \times 10^5 \text{ Mpc}^3$ for the same three cases.

Equation (14) should be regarded as a simple estimate of the volume that needs to be searched. The 2D uncertainty $\langle \delta \Omega^2 \rangle^{1/2}$ was obtained by a Fisher analysis, and represents the solid area of a 2D error ellipse. This equation then gives the volume of a cylinder with a height of $\langle \delta z^2 \rangle^{1/2}$. The arguably more appropriate volume of an ellipsoid whose third semi-axis is $\langle \delta z^2 \rangle^{1/2}$ would be a factor of $4/3$ larger. On the other hand, equation (14) also naively assumes that δz and $\delta \Omega$ are uncorrelated - i.e., it describes an error ellipsoid whose z axis is oriented along the line of sight. The angular position is estimated by *LISA* from the GW signal alone, and is therefore indeed uncorrelated with the radial uncertainties due to cosmology, lensing, or peculiar velocities. However, the luminosity distance estimate from *LISA* itself is strongly correlated with its angular positioning (Hughes 2002), which results in an error ellipse that is ‘tilted’ relative to the line of sight, and has a smaller overall volume than the simple orthogonal product in equation (14) would imply.

We have utilized the correlation matrices for the *LISA* distance and angle estimates given in Table 1 and 2 of Hughes (2002) for $m_1 = m_2 = 10^5 M_\odot$ at $z = 1$ and $m_1 = m_2 = 10^4 M_\odot$ at $z = 7$, to estimate the reduction in the total error volume due to these correlations. Note that this analysis applies only to the *LISA* uncertainties. Among the 11 free parameters in Hughes (2002), the 3D error volume is determined by the parameters related to the spherical coordinates of the sources: $\ln d_L$, $\mu_S = \cos \theta_S$, and ϕ_S . The error volume δV_{tot} quoted in equation (14) above corresponds to $(3/4)$ th of the volume of an ellipsoid whose semi-axes are the *marginalized* errors in spherical coordinates; the true error volume δV_{ell} is that of the ellipsoid described by the full covariance matrix. The ratio $\delta V_{\text{ell}}/\delta V_{\text{tot}}$ depends on the actual position angle (θ_S, ϕ_S) of the source; averaging over all angles, we find $\langle \delta V_{\text{ell}}/\delta V_{\text{tot}} \rangle = 0.31$ (0.20) for masses $m_1 = m_2 = 10^5 M_\odot$ (10^4) at redshift $z = 1$ (7).

If *LISA* errors dominated the total redshift uncertainty $\langle \delta z^2 \rangle^{1/2}$, this implies that the correlations could reduce the mean number of counterparts by a factor of 3–4. However, as discussed above, the total uncertainty is likely going to be dominated by weak lensing errors; hence the inclusion of the

⁷ <http://cas.sdss.org/dr3/en/tools/search/sql.asp>

correlations would reduce the final error volume only by a small factor ($\sim 15\%$). We make no use of this reduction in the results we quote below.

4. QUASAR COUNTERPARTS

To estimate the typical number of quasar counterparts to a specific SMBH merger event, we combine the size, δV_{co} , of the comoving *LISA* error box with the space density of quasars, by integrating over the quasar luminosity function, $\phi(L, z)$:

$$N = b \delta V_{\text{co}} \int_{L_{\text{min}}}^{L_{\text{max}}} dL \phi(L, z), \quad (15)$$

where b accounts for the bias due to the clustering of quasars, and L_{min} and L_{max} are the minimum and maximum quasar luminosities which could be associated to the specific SMBH merger event. We use $L_{\text{min}} = 0.1L_{\text{Edd}}$ and $L_{\text{max}} = 2L_{\text{Edd}}$, where L_{Edd} denotes the Eddington luminosity for the total BH mass. Motivations behind this particular near-Eddington choice are further discussed below.

4.1. Luminosity Function of Quasars

We adopt the standard empirical double power-law fit to the quasar luminosity function of the combined quasar samples from the Two-Degree Field (2dF) and Sloan Digital Sky Survey, with pure luminosity evolution valid for $z < 2.1$ (Richards et al. 2005; Croom et al. 2005). Unfortunately, these surveys extend only to relatively bright magnitudes ($B \lesssim 21$), corresponding to the Eddington luminosity of BHs with mass $M \gtrsim 3 \times 10^7 M_{\odot}$ for $z = 1$, which is above *LISA*'s optimal mass-range. In order to estimate the number of quasar counterparts for lower BH masses, we extrapolate the luminosity function to the faint end.

A limitation of this luminosity function is the simple quadratic fitting formula for the evolution (Richards et al. 2005; Croom et al. 2005), which is only valid for redshifts $z < 2.1$. To avoid these difficulties Madau, Haardt, & Rees (1999) (hereafter MHR) proposed a more complicated empirical fitting formula with three adjustable parameters z_s , ζ , and ξ . These parameters were estimated using high- z quasars, and were improved to include the high-redshift SDSS sample and weak-lensing effects (Wyithe & Loeb 2002). We obtain a luminosity function that is more precise at lower redshifts and is concordant with the redshift scaling by fitting the MHR model to the Richards et al. (2005) luminosity function in the interval $0.5 < z < 2.1$ and keeping the high-redshift asymptote at the Wyithe & Loeb (2002) value. The result is $L^* = 5.06 \times 10^{10} L_{\odot}$, $z_s = 1.66$, $\zeta = 2.6$, and $\xi = 2.8$. Other parameters in the luminosity function that are independent of the evolution are adopted from Richards et al. (2005): $\beta_1 = 1.45$, $\beta_h = 3.31$, and $\Phi_{\text{L}}^* = 1.99 \times 10^{-6} \text{Mpc}^{-3}$.

4.2. Clustering of Quasars

The bias, b , in equation (15) describes the enhancement in the number of quasars around a specific quasar being the potential counterpart, relative to the value for a homogeneous distribution. The clustering depends only weakly on quasar luminosity (Lidz et al. 2005; Adelberger & Steidel 2005). We use the observed autocorrelation function of quasars from the 2dF survey (Croom et al. 2005), $\xi(s) = (s/s_0)^{\gamma}$ for $s > 0.1h^{-1} \text{Mpc}$ (assuming no quasars with a smaller separation), where $s_0 = 5.48h^{-1} \text{Mpc}$ (5.55) and $\gamma = 1.20$ (1.63) for $s <$

TABLE 2
SURVEY CHARACTERISTICS

Survey	M_{min} ($z = 1$) M_{\odot}	Limiting mag	Sky cov. deg ²	Observing
2dF ^a (2QZ,6QZ)	3×10^7	$b_J < 20.85$	750	1997-2002
SDSS ^b (LRG)	2×10^8	$i < 19.1$	7×10^3	1998-2005
Deep2 ^c	5×10^5	$R < 24.5$	4	2002-04
AGES ^d	1×10^7	$R < 21.5$	9	2004-06
DES ^e	7×10^5	$AB < 24.7$	5×10^3	2009-13
LSST ^f	2×10^5	$AB < 26.5$	1.8×10^4	2012

^aTwo-Degree Field, see <http://www.2dfquasar.org/>

^bSloan Digital Sky Survey, see <http://www.sdss.org/>

^cSee <http://deep.berkeley.edu/>

^dAGN and Galaxy Evolution Survey, covers radio, IR, optical, and X-ray bands, see <http://cmb.as.arizona.edu/~eisenste/AGES/>

^eDark Energy Survey, see <http://cosmology.astro.uiuc.edu/DES/> and <http://decam.gnal.gov/>

^fLarge Synoptic Survey Telescope, see <http://www.lsst.org/>

25Mpc ($>25\text{Mpc}$), respectively. The bias is given by the average value of $\langle 1 + \xi(t) \rangle$ over the comoving error box. Assuming that the error box is a cylinder, with height $\delta y = c\delta z/H(z)$ (which is the comoving distance along the line of sight corresponding to the redshift error) and radius $\delta r = \sqrt{\delta V_{\text{co}}/(\pi\delta y)}$ (corresponding to the angular uncertainty of *LISA*):

$$b = \frac{\int_0^{\delta r} 2\pi r dr \int_0^{\delta y} dy (1 + \xi(\sqrt{y^2 + r^2}))}{\int_0^{\delta x} 2\pi r dr \int_0^{\delta y} dy}. \quad (16)$$

We find $b = 1.50$, 1.23, and 1.07, for our best, typical, and worst cases, respectively. The corresponding comoving cylinder heights are $\delta y = 62.5$, 62.9, and 73.8 Mpc, and the cylinder radii are $\delta r = 3.3$, 17.8 and 56.4 Mpc.

5. RESULTS

The main results of this paper are presented in Figure 4, which shows $\langle N \rangle$, the average number of counterparts within the 3D *LISA* error volume, for various total masses M and redshifts z . Recall that we have assumed that the GW event is always accompanied by quasar activity. According to our definition, $\langle N \rangle$ then corresponds to the mean number of quasars that would be found in *LISA*'s error box, *in addition* to the quasar actually associated with the GW source. A straightforward identification of a unique counterpart therefore requires that there be no additional quasars in the error volume and that the EM observation sensitivity goes below the actual counterpart luminosity (so that the presence of fainter quasars can be ruled out). A simple criterion for a reasonable chance not to have any additional counterparts candidates is $\langle N \rangle < 1$.⁸ We find that this simple condition is satisfied in the case of a "typical" event at $z = 1$ with total masses $\sim 4 \times 10^5 M_{\odot}$ or $\sim 8 \times 10^6 M_{\odot}$. At higher redshifts, the average number of potential counterparts will be much larger, due mostly to the increasing weak lensing errors. At $z \gtrsim 3$, even the best case events will typically have at least one additional quasar in their error box. On the other hand, the increase from $z = 3$ to $z = 5$ in the number of quasars located in the error-box is partly mitigated by the drop in the

⁸ One could explicitly consider the probability distribution for N . For example, for a Poisson distribution, the probability for $N = 0$ would be 50/90 percent for $\langle N \rangle = 0.7/0.1$.

abundance of quasars at $z \gtrsim 3$. The three panels of Figure 4 display results for various presumptions of uncertainties. The top panel uses raw, uncorrected weak-lensing errors and the counterpart luminosity is allowed to vary in a broad range $0.1 < L/L_{\text{Edd}} < 2$. The middle panel accounts for a 20% reduction of weak-lensing errors, and the luminosity is restricted to $0.7 < L/L_{\text{Edd}} < 1.3$. The bottom panel shows results for the more conservative scaling of *LISA* errors, $\delta d_L/d_L \propto \Delta T^{-1/2} \times \text{SNR}^{-1}$ and $\partial\Omega \propto \Delta T^{-1} \times \text{SNR}^{-2}$ if $\Delta T < 1$ yr. In all cases at $z \sim 1$, a unique counterpart may be identifiable.

One may also interpret the number of counterparts we compute, $\langle N \rangle$, together with the same simple criterion $\langle N \rangle < 1$, in a somewhat different way: as a means to *test* our hypothesis that *LISA* events are accompanied by bright quasar activity. If our hypothesis is incorrect, then the number of quasars in *LISA*'s error volume should be drawn from the random distribution of quasars on the sky, unrelated to the *LISA* event (excluding the correction due to correlations that we have included in our analysis; although we found this correction to be relatively insignificant). In many configurations, we find $\langle N \rangle \ll 1$, implying a significant probability that *no* bright quasars would be found in *LISA*'s error volume in these cases. If several *LISA* events are indeed found with no such quasar counterparts, it would, by itself, be an important new constraint on the process of binary black hole coalescence.

The identification of counterparts could be aided by a combined analysis of several GW events. Every successful identification yields a very precise direct measurement for the L/L_{Edd} Eddington ratio. Once a statistically significant set of Eddington ratios is acquired, the empirical distribution can be mapped. It is yet unclear whether SMBH mergers are expected to have high-luminosity quasar counterparts. Then, *in case* L/L_{Edd} is in a narrow range, this information can be used to greatly constrain the a priori assumptions on the counterpart's luminosity. As an example, in Figure 4 (middle panel) we consider $L/L_{\text{Edd}} = 1 \pm 0.3$, and find $\langle N \rangle$ to decrease well under 1 in the typical case.

If cosmological uncertainties were to dominate the error budget on a counterpart's redshift, a combined analysis could further improve the robustness of the identification. Indeed, even if each GW event has, by itself, several possible counterparts, each of these counterparts would require a different set of cosmological parameters. As a result, there should be, in general, only a single set of cosmological parameters⁹ that gives a consistent set of counterparts to all of the GW events (Schutz 1986). The counterpart candidates contradicting this concordant set can be discarded. Unfortunately, the error budget is likely to be dominated by the lensing magnification uncertainty. In this case, having multiple events is going to be helpful only if a sufficient number ($\gg 100$) of events are detected to map out the full distribution of magnifications (such a large number of events is not expected; see below).

6. DISCUSSION

6.1. Search Strategy

Different strategies for the search of an electromagnetic counterpart to a *LISA* event can be envisioned. The simplest one would be to search, in an existing survey catalog, for candidates located in the 3D *LISA* error box. We list the char-

⁹ This set, of course, will suffer from the usual degeneracy along the surface of constant $d_L(z, \Omega_\Lambda, \Omega_m, h, w)$ around the fiducial cosmological parameters.

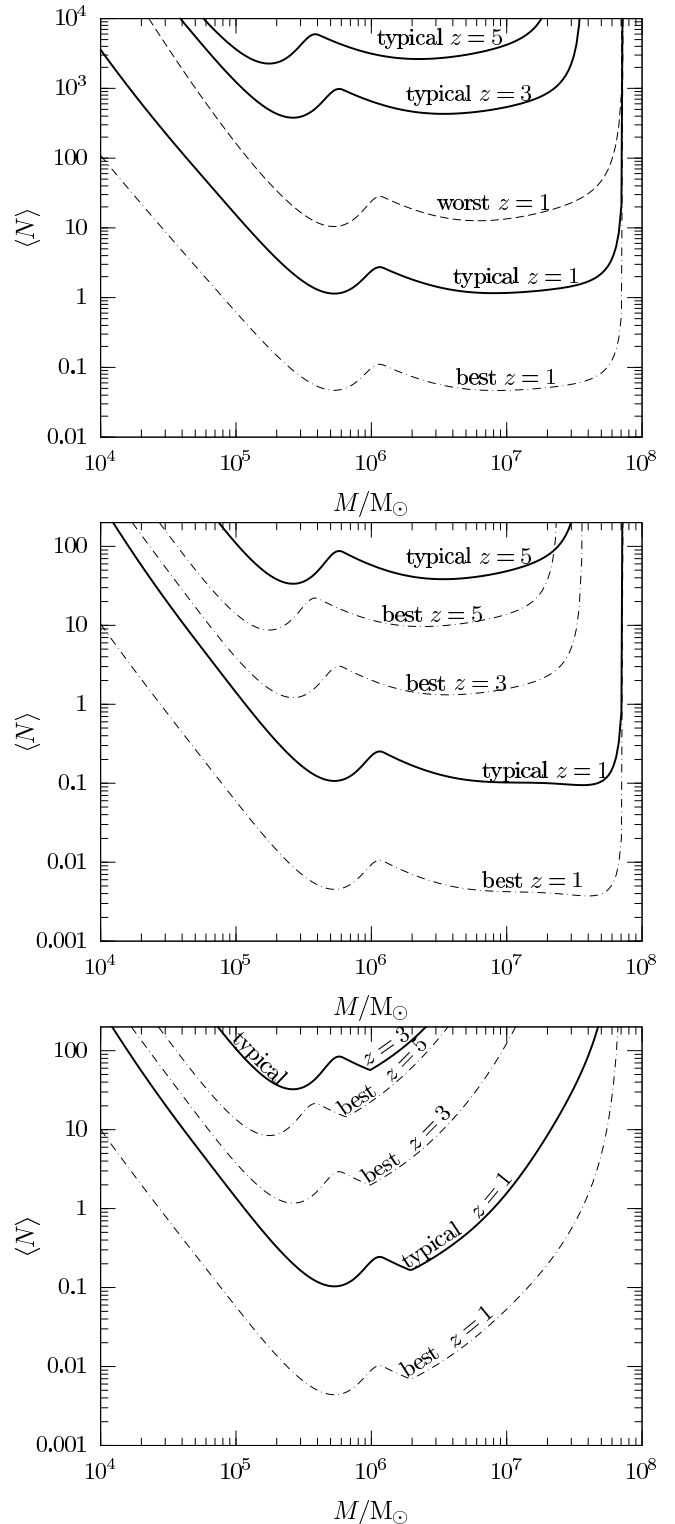


FIG. 4.— The average number of quasars in the three-dimensional *LISA* error volume. The thin dash-dotted, thick solid, and thin dashed curves trace the “best”, “typical”, and “worst” cases, respectively. The low-frequency noise wall for *LISA* is assumed to be at $f_{\text{min}} = 0.03$ mHz. *Top*: Using raw data without any weak-lensing corrections and the counterpart’s luminosity is assumed to be $0.1 < L/L_{\text{Edd}} < 2$. *Middle*: The weak-lensing errors are corrected by 20%, and the luminosity is assumed to be $0.7 < L/L_{\text{Edd}} < 1.3$. *Bottom*: Same as the middle panel, assuming that *LISA* uncertainties scale as $\delta d_L/d_L \propto \Delta T^{-1/2} \times \text{SNR}^{-1}$ and $\partial\Omega \propto \Delta T^{-1} \times \text{SNR}^{-2}$. In most cases at $z \lesssim 1$, a unique quasar counterpart may be identifiable.

acteristics of several deep present and near-future surveys in Table 2. These surveys cover various bands between 400 and 1100nm. In each case, we calculate the minimum mass of the quasar corresponding to the magnitude limit of the survey, provided that the quasar is shining at the Eddington luminosity. For the quasar spectrum we use Madau, Haardt, & Rees (1999) and follow Madau (1995) to account for the Lyman series line blanketing and photoelectric HI absorption to obtain the apparent luminosity. The portion of the sky covered and scheduled operation times are also given. The most promising (deepest and largest sky coverage) among the planned surveys is that from the LSST, scheduled for the same time as *LISA*.

A second strategy would be to design a survey specifically aimed at identifying the counterparts of well-localized *LISA* events, by observing in detail the 2D angular error box provided by *LISA* and looking for the expected counterparts. The time domain may come to play an important role in the strategy of this type of surveys. Indeed, for some of the events, one may have, from the *LISA* data-stream, a reasonably good idea of the location on the sky of the SMBH binary prior to coalescence. For instance, Holz & Hughes (2005) estimate that this knowledge may be available with reasonable accuracy about a day in advance. One would then be able to monitor any unusual photometric variability associated with the violent SMBH merger in this area somewhat before, during and after the coalescence. Surveying the area long (i.e. months or years) after the coalescence may also prove useful in discovering the counterpart and/or monitoring the viscous evolution of any gas surrounding the SMBH merger remnant (Milosavljevic & Phinney 2005). The time domain may thus greatly facilitate the identification of a unique electromagnetic counterpart to some *LISA* events, even in cases when many counterpart candidates otherwise exist in the 3D error box.

6.2. Uncertainties in the Analysis

Throughout the analysis of *LISA* uncertainties, we focused on equal mass binaries. With this simplifying assumption, it was possible to derive approximate scalings as a function of total mass and relate them to the calculations of Vecchio (2004) for $m_1 = m_2 = 10^6 M_\odot$. We also find good agreement with the recent calculations of Holz & Hughes (2005) for a variety of equal-mass combinations. For unequal masses, the GW signal-power depends to leading order on the simple combination $\mathcal{M} = \mu^{3/5} M^{2/5}$, allowing a straightforward extension of our scaling arguments to more general mass ratios.

As mentioned above, our results depend on the *LISA* sensitivity curve at low frequencies. In particular, the relationship between the arrival frequency $f_a(M_z, \Delta T)$, the final frequency $f_{\text{isco}}(M_z)$, and the *LISA* minimum frequency noise wall f_{min} determines the maximum possible observation time for the in-spiral. The exact value of f_{min} is currently assumed to lie between 0.1 and 0.03mHz. Figure 4 assumes $f_{\text{min}} = 0.03\text{mHz}$. In this case, at $z = 1$, a $\Delta T = 1\text{yr}$ observation of the in-spiral phase is possible for $M < 2 \times 10^6 M_\odot$ but for larger masses, the maximum possible observation time becomes shorter than a year. We have also computed the number of quasars in the 3D *LISA* error box for the higher value of $f_{\text{min}} = 0.1\text{mHz}$. We find a significant increase in this number at the high-mass end (i.e. for $M \sim 10^7 M_\odot$), but the results are essentially unaffected for lower mass SMBHs.

An important assumption in our analysis is the near-Eddington luminosity of the quasar counterparts associated with *LISA* events. While this assumption is difficult to justify from first principles, it is the luminosity expected if SMBH

accretion occurs in a regime which is not supply-limited. Observationally, the Eddington ratio of quasars, L/L_{Edd} , can be inferred, leading to values from 0.1 to $\gtrsim 1$, with higher values at large redshifts (e.g. Kaspi et al. 2000; Vestergaard 2004; Woo & Urry 2002). This ratio has been determined for a handful of lower mass SMBHs in AGNs and these sources have been found to cluster around $L/L_{\text{Edd}} \sim 1$ as well (Greene & Ho 2004). Recent work by Kollmeier et al. (2005) and Hopkins et al. (2005) both suggest L/L_{Edd} is typically around 1/3.

The restricted luminosity range $0.1 < L/L_{\text{Edd}} < 2$ assumed in our analysis effectively serves as a 4th (“brightness”) dimension, complementing the three-dimensional geometrical error volume provided by *LISA*. According to Table 1, for a given event, the mass estimate provided by *LISA* is typically very accurate. Therefore, it is through the range of acceptable Eddington ratios that the integration bounds in equation (15) change. Since the luminosity function decreases rapidly with L , the integral is dominated by the lower bound and is largely independent of L_{max} . We chose $L_{\text{max}} = 2L_{\text{Edd}}$ for concreteness. When modifying the lower bound from $L_{\text{min}} = 0.1L_{\text{Edd}}$ to $L_{\text{min}} = 1.0L_{\text{Edd}}$ or $L_{\text{min}} = 0.01L_{\text{Edd}}$, for instance, we find that the number of quasars present in the 3D *LISA* error box changes by a factor of 0.1 and 5, respectively.¹⁰ Obviously, our need to extrapolate the quasar luminosity function below the minimum value constrained by the observations is an additional important source of uncertainty in our analysis, but one that will be addressed well by future generations of surveys (Table 2).

In a recent study, Hennawi et al. (2005) have found a large number of small-separation quasars, implying an order-of-magnitude increase in the quasar auto-correlation on scales $\lesssim 200h^{-1}$ kpc. However, the dimensions of the error volume as we estimated it is generally much larger (~ 3.3 Mpc even in our best case). As a result, the average number of counterparts is changed by a negligible factor by this small-scale auto-correlation: 8.3×10^{-3} , 3.7×10^{-4} , and 3.3×10^{-5} in the best, typical, and worst case *LISA* errors. Increasing the correlation by an order of magnitude out to a scale of $500h^{-1}$ kpc would still cause at most a 6% increase in the mean number of quasars in the best case. Hennawi et al. (2005) do not find an increase in the correlation beyond $\sim 500h^{-1}$ kpc scales. We note that our inability to identify the correct counterpart from among any rare ultra-small-separation candidates would not degrade cosmological parameter estimations significantly. One may also argue that such close-separation binary quasars would better represent a ‘precursor’ stage in the evolution of the two black holes towards an eventual coalescence. If so, one would not expect them to be associated with GW events, and they may in fact be anti-correlated with such events.

Throughout this paper, we have focused on optical quasars as plausible counterparts to GW events. It would be interesting to repeat our analysis using other types of “electromagnetic objects” that may be associated with SMBH coalescences. For example, even if gas accretion leads to prodigious energy output in radiation, the optical light of the quasar may be obscured by the intervening gas and dust near the galactic nucleus. In these cases, the GW events may be more commonly associated with X-ray quasars (e.g. Milosavljevic & Phinney 2005), or with ultraluminous infrared galaxies (e.g. Thompson et al. 2005). As these sources

¹⁰ The change is explained by the asymptotic form of the luminosity function $\Phi(L) \propto L^{-1.45}$ for low L .

are also relatively rare, unique counterparts may be identifiable if such objects typically accompany GW events.

6.3. Implications: Black Hole Astrophysics

A successful identification of a quasar counterpart to a *LISA* event would provide powerful diagnostics on the physics of SMBH gaseous accretion and the associated radiation. The masses and spins of the two BHs before merger can be directly determined from the GW signal, from which the mass and spin of the remnant BH follows at some precision. In some cases (e.g. Hughes & Menou 2005), the remnant BH could also be observed by *LISA* during the post-merger ring-down phase, which would constrain its mass and spin directly. The orientation of the orbital plane of the BH binary before merger would be measured as well. All of these parameters are generally unknown for quasars detected only via traditional electromagnetic techniques.

The observation and monitoring of quasar counterparts to *LISA* events may thus offer us some of the best laboratories for the study of AGN physics. First, the Eddington ratio can be measured to high accuracy (limited only by photometric errors and bolometric corrections), since *LISA* estimates for the BH masses are extremely precise by astronomical standards (see Tab. 1). Second, if the quasar accretes at or near the Eddington limit, given its Eddington ratio, one may be able to set a useful lower limit on the radiative efficiency of its accretion flow. If it is in excess of the canonical 10% value, it will provide an interesting empirical test of the physics of accretion onto a spinning BH, with a spin directly constrained by the GW measurement. Third, the counterpart could be monitored for years following the merger to follow the viscous evolution of the gaseous disk and thus clarify its role in the SMBH coalescence process. Fourth, it is expected that the gas disk will be forced in the orbital plane of the pre-merger binary by the Bardeen-Peterson effect (Milosavljevic & Phinney 2005). Knowing the disk orientation could thus offer tests of the geometry of quasar emission and obscuration (even after the merger, given the expected spin of the remnant). It may also be possible to further develop diagnostics related to the geometry of a jet, if present.

6.4. Implications: Cosmology

The successful identification of an EM counterpart to a GW event could, in principle, open the way to use them as “standard sirens” to probe the background cosmology (Schutz 1986), analogously to the Ia SNe standard candles (Holz & Hughes 2005). The precision on the cosmological model can, however, be improved only if the $d_L(z)$ function is determined to a higher accuracy than it can be already guessed from other data that exists when *LISA* is operational. As an example, we have assumed here to have available the uncertainty from the combined datasets from two future projects, *Planck* and LSST. We have found that the major obstacle against a dramatic improvement on cosmology is the gravitational lensing of intervening matter along the line of sight to a *LISA* source. In the weak-lensing limit, the r.m.s. magnification of a source at $z = 2$ is 12%, leading to a luminosity distance error of 6%. Dalal et al. (2003) have shown that galaxy shear maps can be used to correct weak-lensing distortion, but only a 20% relative improvement can be achieved, so that $\delta d_L/d_L = 5\%$. We suggest alternatively that correcting for

the contribution of the known distribution of intervening matter might improve weak lensing uncertainties by another 20%. Furthermore, the weak lensing uncertainty can be overcome if a large sample of sources is available when fitting $d_L(z)$, mapping out the magnification distribution. Using a number K of merger events along with uniquely identified counterparts, the lensing error reduces approximately as $1/\sqrt{K}$ (although the actual improvement will be less pronounced, due to a non-Gaussian tail of high magnifications; Wang, Holz, & Munshi 2002; Holz & Linder 2004). To reach the *Planck* + LSST level of $\delta d_L/d_L = 10^{-3}$, we find that $K > 100$ events would be required.

Is such a large number of merger events, with uniquely determined electromagnetic counterparts, expected from the *LISA* data-stream? Monte-Carlo simulations of SMBH merger trees generally indicate *LISA* event rates from $\sim 20\text{--}0.5\text{yr}^{-1}$ for masses $M_{\text{BH}} \lesssim 10^7$ at $z \sim 1$ (Menou, Haiman, & Narayanan 2001; Sesana et al. 2004; Enoki et al. 2004). Detecting a total of $K = 100$ would be barely possible during a 3-year *LISA* mission lifetime, only allowing a marginal test of the concordance of cosmological parameters with standard sirens. In addition, most of these events may be expected to involve SMBHs at the low-mass end (i.e. $\lesssim 10^5 M_\odot$; Menou 2003; Sesana et al. 2004), which are not ideal for unique counterpart identifications (see Fig. 4). However, large uncertainties remain on the expected event rate. For example, Islam, Taylor, & Silk (2004) predict much larger rates, which could open up the possibility of a statistical analysis, folding in the expected weak lensing magnification distribution.

7. CONCLUSIONS

In this paper, we have considered the possibility that SMBH-SMBH mergers, detected as gravitational wave sources by *LISA*, are accompanied by gas accretion and quasar activity with a luminosity approaching the Eddington limit. Under this assumption, we have computed the number of quasar counterparts that would be found in the three-dimensional error volume provided by *LISA* for a given GW event. We found that weak lensing errors exceed other sources of uncertainties on the inferred redshift of the electromagnetic counterpart and increase the effective error volume by nearly an order of magnitude. Nevertheless, we found that for mergers between $\sim (4 \times 10^5 - 10^7) M_\odot$ SMBHs at $z \sim 1$, the error box may contain a single quasar with a B-band luminosity $L_B \sim (10^{10} - 10^{11}) L_\odot$. This would make the identification of unique electromagnetic counterparts feasible, allowing precise determinations of the Eddington ratio of distant accreting SMBHs, and providing an alternative method to constrain cosmological parameters.

We thank Dan Holz, Scott Hughes, Szabolcs Márka, and Merse E. Gáspár for useful discussions. We are grateful to Sheng Wang for providing the Fisher matrices. Z. H. was supported in part by NSF through grants AST-0307200 and AST-0307291, by NASA through grant NNG04GI88G, and by a György Békésy Fellowship from the Hungarian Ministry of Education. Z. F. acknowledges support from OTKA through grant nos. T037548, T047042, and T047244.

REFERENCES

- Barack, L. & Cutler, C. 2004, *Phys. Rev. D*, 69, 082005
- Barnes, J. E., & Hernquist, L. 1992, *ARA&A*, 30, 705
- Begelman, M. C., Blandford, R. D., & Rees, M. J. 1980, *Nature*, 287, 307
- Berti, E., Buonanno, A., & Will, C. M. 2005a, *Phys. Rev. D*, 71, 084025
- Berti, E., Buonanno, A., & Will, C. M. 2005b, *Class. Quant. Grav.*, 22, 943
- Cen, R., & Ostriker, J. P. 2000, *ApJ*, 538, 83
- Croom, S. M. et al. 2005, *MNRAS*, 356, 415
- Dalal, N., Holz, D. E., Xuelei, C., & Frieman, J. A. 2003, *ApJ*, 538, L11
- Danzmann 2004, 5th Int'l *LISA* Symp., http://www.rssd.esa.int/SP/SP/docs/LISASymposium/K.Danzmann/KD_LISASymp04.pdf
- Enoki, M., Inoue, K. T., Nagashima, M., & Sugiyama, N. 2004, *ApJ*, 615, 19, astro-ph/0502529
- Escala, A., Larson, R. B., Coppi, P. S., & Mardones, D. 2004, *ApJ*, 607, 765
- Fan, X. et al. 2001, *AJ*, 121, 54
- Fang, T., & Canizares, C. R. 2000, *ApJ*, 539, 532
- Gould, A., & Rix, H.-W. 2000, *ApJ*, 532, 29
- Greene, J. E., & Ho, L. C. 2004, *ApJ*, 610, 722
- Haiman, Z., & Loeb, A. 1998, *ApJ*, 503, 505
- Haiman, Z., & Menou, K. 2000, *ApJ*, 531, 42
- Hamana, T., Kayo, I., Yoshida, N., Suto, Y., & Jing, Y. P. 2003, *MNRAS*, 343, 1312
- Hennawi, J. F. et al. 2005, *AJ*, submitted, astro-ph/0504535
- Holz, D. E. & Hughes, S. A. 2005, *ApJ*, 629, 15
- Holz, D. E., & Linder, E. V. 2004, *AAS Meeting* 205, 131.02, astro-ph/0412173
- Hopkins, P. F., Hernquist, L., Cox, T., Robertson, B., Di Matteo, T., & Springel, V. 2005, *ApJ*, submitted, astro-ph/0506398
- Hu, W., & Haiman, Z. 2003, *Phys. Rev. D*, 68, 063004
- Hughes, S. A. 2002, *MNRAS*, 331, 805
- Hughes, S. A., & Menou, K. 2005, *ApJ*, 623, 689
- Islam, R. R., Taylor, J. E., & Silk, J. 2004, *MNRAS*, 354, 629
- Kaspi, S., Smith, P. S., Netzer, H., Maoz, D., Jannuzi, B. T., & Giveon, U. 2000, *ApJ*, 533, 631
- Kauffmann, G., & Haehnelt, M. 2000, *MNRAS*, 311, 576
- Kauffmann, G., & Haehnelt, M. 2002, *MNRAS*, 332, 529
- Kollmeier, J. A. 2005, astro-ph/0508657
- Lidz, A., Cox, T. J., Hernquist, L., & Robertson, B. 2005, *ApJ*, submitted, astro-ph/0507361
- Madau, P. 1995, *ApJ*, 441, 18
- Madau, P., Haardt, F., & Rees M. J. 1999, *ApJ*, 517, 648
- Menou, K. 2003, *Class. Quantum Grav.*, 20, 37
- Menou, K., & Haiman, Z. 2004, *ApJ*, 615, 130
- Menou, K., Haiman, Z., & Narayanan, V. K. 2001, *ApJ*, 558, 535
- Milosavljevic, M., & Phinney, E. S. 2005, *ApJ*, 622, L93
- Perna, R., & Loeb, A. 1998, *ApJ*, 503, L135
- Richards, G. T. et al. 2005, *MNRAS*, 360, 839
- Schutz, B. F. 1986, *Nature*, 323, 310
- Sesana, A., Haardt, F., Madau, P. & Volonteri, M. 2004, *ApJ*, 611, 623
- Small, T. A., & Blandford, R. D. 1992, *MNRAS*, 259, 725
- Smith, R. E. et al. 2003, *MNRAS*, 341, 1311
- Spergel, D. N. et al. 2003, *AJS*, 148, 175
- Tegmark, M. 2004, *Phys. Rev. D*, 69, 103501
- Thompson, T. A., Quataert, E. & Murray, N. 2005, *ApJ*, 630, 167
- Vecchio, A. 2004, *Phys. Rev. D*, 70, 042001
- Vestergaard, M. 2004, *ApJ*, 601, 676
- Volonteri, M., Madau, P., Quataert, E. & Rees, M. J. 2005, *ApJ*, 620, 69
- Wang, Y., Holz, D. E., & Munshi, D. 2002, *ApJ*, 572, L15
- Wang, S., Khoury, J., Haiman, Z., & May, M. 2004, *Phys. Rev. D*, 70, 123008
- White, M., & Hu, W. 2000, *ApJ*, 537, 1
- Woo, J.-H., & Urry, C. M. 2002, *ApJ*, 579, 530
- Wyithe, J. S., & Loeb A. 2002, *ApJ*, 577, 68
- Wyithe, J. S., & Loeb A. 2003, *ApJ*, 595, 614